Flow Characterisation of a Two-Phase Natural Circulation Loop

PT Senda[a] and RT Dobson[b]

Received 28 February 2018, in revised form 13 December 2018 and accepted 17 December 2018

Abstract: The focus of this paper is the experimental and theoretical analysis of the transient behaviour of a two-phase flow natural circulation heat transfer loop using water as the working fluid. The loop is a rectangular vertically orientated 32 mm inside diameter copper pipe of height 7 m and width 8 m. To theoretically simulate the loop, the working fluid is discretized into a series of one dimensional control volumes. When applying the conservation of mass, momentum and energy, and suitable property functions to each control volume, a series of time dependent partial differential equations is generated. Equations are then solved using an explicit finite difference method computer program created in Q-Basic64 programming language. A separated two-phase flow model is applied with frictional multipliers and vapour-liquid void fraction correlations similar to those originally suggested by Martinelli. One vertical side of the loop is heated using electrical heating elements and the other vertical side is cooled using a series of pipe-in-pipe heat exchangers. Transparent pipe lengths are inserted in the loop in order to observe the two-phase flow patterns. The loop is operated in single to two phase operating mode. A reasonable correlation between the experimental and theoretical simulations is found thereby validating the theoretical model. It is concluded that the theoretical model adequately represents the actual transient and heat transfer behaviour of the loop.

Additional keywords: Natural circulation, heat transfer loop, transient flow, two-phase flow, explicit finite difference method, flow patterns.

Nomenclature

Roman

a	acceleration,[m/s^2]
A	Area, [m^2]
A_x	cross sectional area, [m^2]
A_z	heat transfer area, [m^2]
C_f	coefficient of friction
d	diameter, [m]
G	Force due to gravity, [N]; mass flux, [kg/m^2], mass velocity, [kg/m^{2}s]
h	height, head, [m]
m	mass, [kg]
$\dot{m}$	mass flow rate, [kg/s]
N	number
P	pressure, [Pa]
$\wp$	perimeter, [m]
$\dot{Q}$	heat flow rate, [W]
$\dot{Q}'''$	heat transfer rate per unit volume, [W/m^3]
Re	Reynolds number $Re = \rho v d/\mu$
S	Slip factor; Suppression factor
T	temperature, [K, °C]
t	time, [s]
u	specific internal energy, [J/kg]
v	velocity, [m/s]
V	volume, [m^3]
x	mass fraction, $m_{vapour}/(m_{vapour} + m_{liquid})$; displacement, [m]
X	Martinelli parameter
z	distance, [m]
z_{minor}	minor losses
a	times new Roman 10 [unit]
A	alphabetical order [unit]
B	next symbol [unit]

Greek

α	void fraction, $\alpha = V_g/(V_g - V_l)$
θ	inclination angle, [rad]
μ	dynamic viscosity, [Ns/m^2]
ρ	density, [kg/m^3]
σ	surface tension [N/m]
σ	Stefan-Boltzmann constant, [W/m^{2}K^4]
τ	shear stress, [N/m^2]
ϕ^2	two-phase frictional multiplier

Superscripts

t	time
Δt	time step

Subscripts

e	electrical; equivalent
exp	experimental
f	saturated liquid; friction
g	gas
l	liquid
atm	atmospheric
v	vapour
lo	liquid only
tot	total
th	theoretical
i	ith control volume or element
h	hydraulic; wetted perimeter
in	inlet
out	outlet
minor	minor losses
w	water, wall
tank	tank

Abbreviations

BL	Bottom Left
BR	Bottom Right
E&H	Endress and Hauser

a. Department of Mechanical Engineering, Cape Peninsula University of Technology, Bellville, South Africa. ptsenda@gmail.com
b. Department of Mechanical Engineering, University of Stellenbosch, Stellenbosch, South Africa. rtd@sun.ac.za

https://doi.org/10.69694/2309-8988/v34a9

F Friction
G Gravity
H Heater
HBM Hottinger Baldwin Messtechnic
HE Heat Exchanger
M Mass
MF Momentum flux
P Pressure
SF Slip Factor
TL Top Left
TR Top Right

1 Introduction

A natural circulation loop is a closed thermosyphon loop that transfers energy from a heat source to a separate heat sink over a relatively long distance without the use of any mechanically moving devices. This process is also called a *passive* system as no active components (for example a pump) are needed. The process is also *self-controlling*; as the temperature difference between the heat source and the sink increases, so too do the flow rate and heat transfer rate.

Thermosyphon loops are used in many technological applications. Notably solar heaters, air conditioning and ventilation, nuclear power plants and thermal management of electrical and electronic devices. In the nuclear industry this thermosyphonic flow process is considered a passive system and integrally safe. This makes it suitable for use in reactor safety cooling, where reliability and safety are of paramount importance. For instance, they may be used in high temperature reactors in the reactor cavity cooling system (RCCS). The objective of a RCCS is to transfer the *afterheat* from the reactor cavity to an outside environment or ultimate heat sink in case of a loss of primary coolant. Thereby ensuring the thermal integrity of the fuel, core vessel and critical equipment within the reactor cavity concrete containment structures [1].

Figure 1 depicts a number of natural circulation loops. They may be termed as *integrated* (a), *separated* (b), *closed* (c), *closed loop* (d) and *heat pipe* (e). A natural circulation system may be said to be integrated when the circulation takes place entirely within a single containment vessel. For example the hot reactor core coolant flows upward inside the riser and then downwards on the outside where it is cooled by the secondary flow through the heat exchanger positioned between the riser and the reactor vessel [2], as also shown schematically in figure 1(a). This paper specifically considers only a closed-looped thermosyphon-type as depicted in figure 2; with the left side of the loop heated using electrical heating elements (to simulate the reactor afterheat) and the right side water-cooled using pipe-in-pipe heat exchangers (to simulate the heat sink).

1.1 Motivation

Because natural loop thermosyphons are a safe and reliable method of transferring heat and do not need any mechanical devices to operate, they are suitably used as passive reactor cooling options in the nuclear industry. Indeed the International Atomic Energy Agency (IAEA) notes [3] that passive safety systems are the preferred method and should be used wherever possible. It is thus important to have a reliable analytical performance prediction procedure to assist in the design of such systems. A computer program was therefore developed in Q-Basic64 to numerically solve the theoretically derived mathematical simulation model. It was formulated using the separated two-phase flow to capture the thermal-hydraulic transient behaviour of the natural circulation cooling loop.

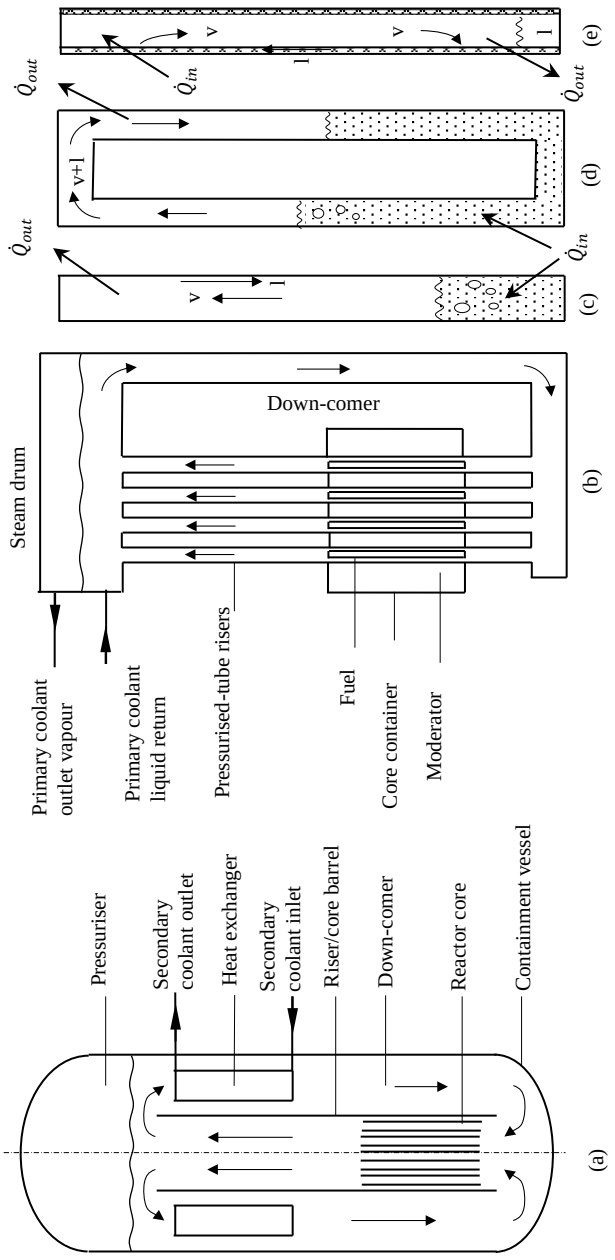

Figure 1 Natural circulation loops, integrated (a), separated (b), closed (c) and looped thermosyphon-type heat pipe (d) respectively, and a surface tension capillary structure or wicked heat pipe (e)

1.2 Objectives

The significance of this paper is to present an investigation into the use of a separated two-phase flow model to capture the transient and dynamic behaviour of the flow and heat transfer in a water charged natural circulation loop, similar to the one shown in figure 2. To date no such approach has been applied to such a large thermosyphon-type heat pipe loop. Single phase and two-phase operating conditions are to be

https://doi.org/10.69694/2309-8988/v34a9

considered. The transition from single to two-phase flow and *vice versa* is also considered.

1.3 Approach

In order to achieve the objectives of this paper as set out in section 1.2, the approach adopted is given as follows. A brief literature survey that is presented in section 2 identifies literature relating to natural circulation and two-phase flow in natural circulation loops. Section 3 gives a detailed formulation of the theoretical model developed and used to simulate and capture the thermal-hydraulic performance of the loop with the help of Q-Basic64 computer program. Section 4 describes the experimental set-up and procedures. Section 5 gives a few typical results, both theoretical and experimental. A discussion leading to conclusions is given in section 6, whilst section 7 gives a summarising final conclusion and recommendations for future work.

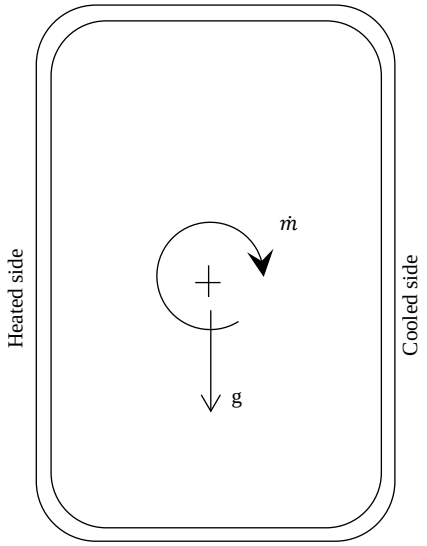

Figure 2 Closed natural circulation loop

2 Background literature

Thermosyphon technology was formally used by Perkin [4] in the 1830's and in what was for more than a century known as a "Perkins boiler". Other applications included baking bread whereby the heat from fire was transferred to a separated oven using Perkins-type thermosyphons. Thermosyphons also found application in early motor car engines that were cooled using natural circulation of water to transfer the heat from the engine to the air-cooled radiator.

Many geometric configurations of closed loop thermosyphons have been studied. Some of the shapes considered have been *circular toroidal* [5], arbitrary toroidal [6], conjugate [7], double thermosyphon [8], multi-channel [9] and rectangular [10, 11]. Vijayan et al. [12] gives a number of useful references and Greif [13] gives a comprehensive review of natural circulation loops as of up to about 1990. Vijayan and Nayak give a review [14] and comprehensive discussion [15] of what they call *flow instabilities* in natural circulation systems. Bhattacharyya [16] gives a thorough review of recent advances in two-phase natural circulation loops where general modelling strategies were reported and compared.

This paper however continues from essentially three works; by Dobson [17] in which the transient response of a closed loop thermosyphon was investigated, by Ruppersberg [18] and by Sittmann [19] in which loops suitable for a reactor cavity cooling system of a pebble bed modular reactor was investigated. Ruppersberg's loop was 1.8 m high, 1.6 m wide and 25.4 mm diameter, and Sittmann considered a one-third-height scale model and is shown in figure 3. The loop is 7 m high and 8 m wide and 32 mm inside diameter. Electrical heating elements are attached to 50 mm wide and 10 mm thick fins (as shown in the insert in figure 9), and is water-cooled using pipe-in-pipe heat exchangers. These three investigations could essentially be regarded as being based on the *homogeneous* two-phase flow model as defined in basic two-phase texts [20], [21] and [22], applied to a rectangular loop. The homogeneous flow model requires an empirically determined friction factor. In this paper we consider the separated two-phase flow model; it requires an additional empirically determined factor namely the void fraction α to capture the transient and dynamic performance of the loop.

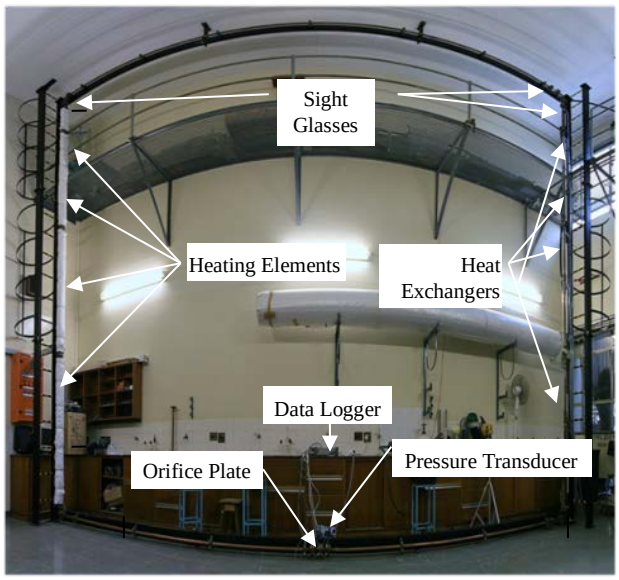

Figure 3 Sittmann's experimental setup (Sittmann, 2010)

The flow in a natural circulation loop as it is heated up as a function of time exhibits certain transient and periodic oscillatory flow behaviour. To analyse this, it is important to predict the pressure difference across a flow meter as a function of time. Vijayan *et al*. [23], give an experimentally determined stability map for a ϕ9.1 diameter pipe, suitable for flow instabilities prediction. The use of the words *instability* and *stability*-map are generally used by researchers to characterise this detailed oscillatory behaviour [15].

For the two-phase flow in vertical round tube, Whalley [20] gives the possible observed flow regimes. He regrouped them in five types where at low quality the bubbly flow is observed. The flow then changes to plug flow, churn flow, annular flow and finally wispy-annular with more heat input into the system.

3 Theory

Having a clear definition of the loop (as shown in figure 3) the systems is discretized into a number of control volumes as schematically depicted in figure 4. For a separated two-

phase flow model each cylindrical control volume in turn is divided into a liquid and gas or vapour portion as shown in figure 5. The equations of change (conservation of mass, momentum and energy) with suitable properties functions are applied to each control volume. To do this however the following assumptions and simplifications needed to be made.

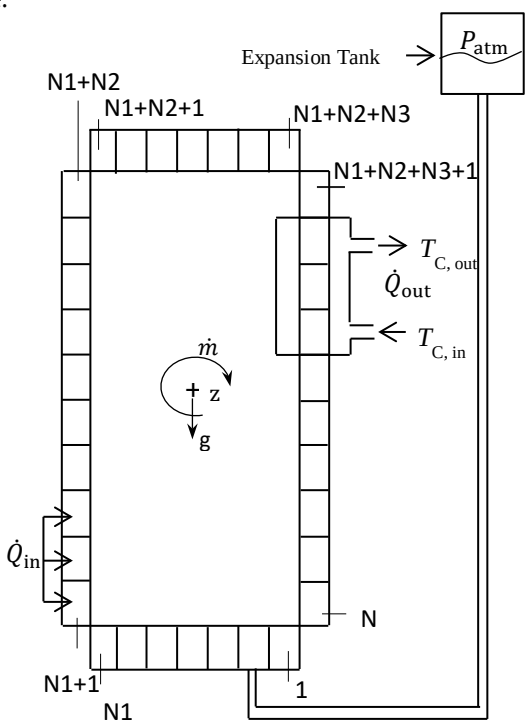

Figure 4 Discretisation schematic of the natural circulation theoretical thermosyphon loop

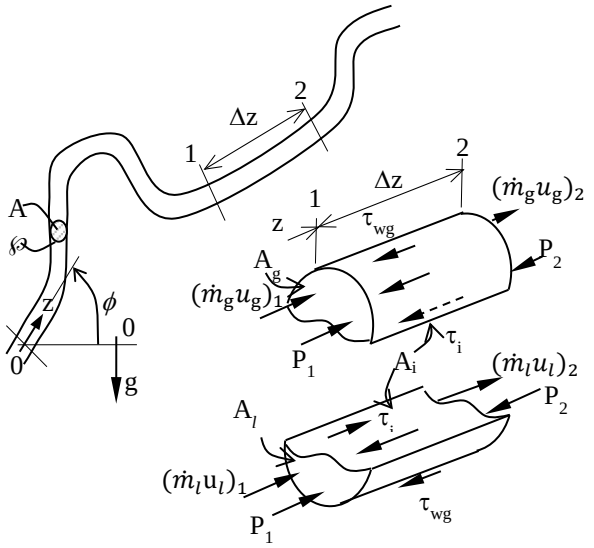

Figure 5 One-dimensional separated flow conservation of momentum control volumes for two-phase fluid flow in a pipe

The mathematical model was developed subject to the following assumptions:

1. The cylindrically-shaped control volumes are one-dimensional; that is at any cross-section area along the axis of the flow $\dot{m} = \int_0^R \rho v 2\pi dr = \rho v A$, where $A = \pi R^2$.
2. At any instant in time the mass flow rate in the loop is independent of its position in the loop; this implies that at any instant in time that $\frac{\partial \dot{m}}{\partial z} = 0$ but $\frac{\partial \dot{m}}{\partial t} \neq 0$. This condition is often called quasi-static or quasi-equilibrium.
3. At any cross-section both the liquid and vapour phases are in thermodynamic equilibrium with each other.

The *separated two-phase flow model* [20, 21] is used to represent the properties and behaviour of the control volumes containing both the liquid and steam. Figure 5 shows a one-dimensional separated flow control volume.

A separated two-phase model requires for a control volume that:

$$m = m_v + m_l, \dot{m} = \dot{m}_v + \dot{m}_l, \dot{m}_v = \rho_v v_v A_v \text{ and } \dot{m}_l = \rho_l v_l A_l \quad (1)$$

a mass fraction

$$x = \frac{m_v}{m_v + m_l} = \frac{\dot{m}_v}{\dot{m}_v + \dot{m}_l} \quad (2)$$

and a density

$$\rho = \alpha \rho_v + (1 - \alpha)\rho_l \quad (3)$$

where the *void fraction* α is defined by

$$\alpha = \frac{V_v}{V_v + V_l} = \frac{\dot{V}_v}{\dot{V}_v + \dot{V}_l} = \frac{A_v}{A_v + A_l} \quad (4)$$

The void fraction may also be expressed as

$$\alpha = \left(1 + \frac{v_v}{v_l}\frac{1-x}{x}\frac{\rho_v}{\rho_l}\right)^{-1} \quad (5)$$

The ratio v_v/v_l is termed *slip factor* and needs to be given as an experimentally correlated expression. One such correlation (Chisholm, 1983) for the void fraction for a two-phase water system is given by the Lockart-Martinelli correlation as

$$\alpha = (1 + 0.28X)^{-1} \quad (6)$$

where X, the so-called Martinelli parameter, is given as

$$X = 1 + \left(\frac{\rho_v}{\rho_l}\right)^{0.5}\left(\frac{\mu_l}{\mu_v}\right)^{0.5}\left(\frac{1-x}{x}\right)^{0.875} \quad (7)$$

Further, an experimentally determined correlation for a so-called frictional multiplier ϕ is needed. One such correlation, the *Lockart-Martinelli liquid only two-phase frictional multiplier* is given as

$$\phi_{lo}^2 = \left(1 + \frac{20}{X} + \frac{1}{X^2}\right)(1 - x)^{1.75} \quad (8)$$

In this case it implies that there is a *liquid only* velocity defined as $v_{lo} = \frac{\dot{m}_v + \dot{m}_l}{\rho_l(A_v + A_l)}$ and with a *liquid only* Reynolds number given as $Re_{lo} = \rho_l\left(\frac{\dot{m}_v + \dot{m}_l}{\rho_l(A_v + A_l)}\right) d_h/\mu_l = \dot{m}'' d_h/\mu_l$ where $d_h = 4A/\wp\Delta z$, $\wp$ being the wetted perimeter and $\dot{m}'' = \dot{m}/A$ is the mass flux. These definitions allow the shear stress to be expressed in terms of a *liquid-only shear stress* τ_{lo} and a *two-phase liquid-only frictional multiplier* ϕ_{lo}^2 as $\tau = \tau_{lo}\phi_{lo}^2$ where $\tau_{lo} = C_{flo}\frac{\dot{m}^2}{2\rho_l A^2}$. A Blasius-type *liquid-only* coefficient of friction (for a smooth tube) is assumed as $C_{flo} = 0.079 Re_{lo}^{-0.25}$ for turbulent flow and $C_{flo} = 16/Re_{lo}$ for laminar flow, and to ensure non-division, by zero if $Re_{lo} < 1$, $C_{flo} = 16$ for laminar flow. Note that the Reynolds number of 1181 is considered for the transition from turbulent to laminar flow, and vice versa to ensure that

the coefficient of friction C_{flo} is a continuous of Re_{lo} , if deemed appropriate. Maybe one would want to build in some "extra complexity" into the simulation model by introducing some sort of hysteresis, assuming for example, that laminar flow becomes turbulent at *Re* = 2300 and that turbulent flow changes to laminar flow at *Re* = 1800.

3.1 Conservation equations

Having now made the assumptions as laid out above, the equations of change may now be applied. This section deals with the equation of change obtained by applying the general statements of the conservation of mass, momentum and energy to each control volume of the discretised system, in order to develop differential equations for theoretical algorithm computer simulation.

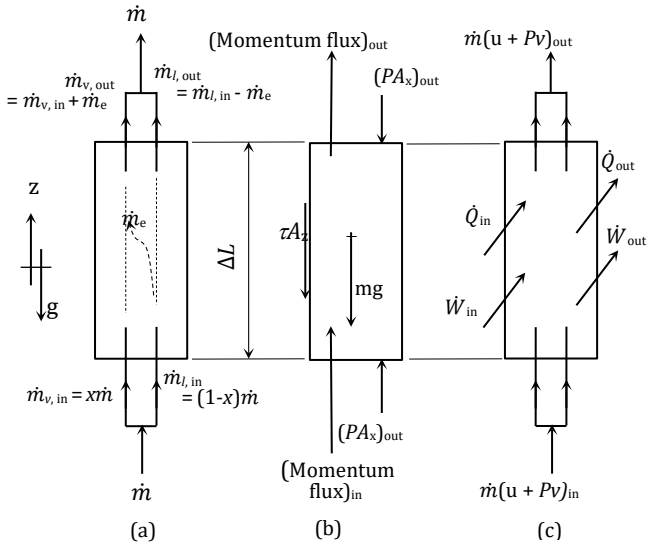

Figure 6 Conservation of (a) mass, (b) momentum and (c) energy as applied to a representative control volume

In order to determine how much mass is transferred to or from the expansion tank, the conservation of mass is applied to the control volume as shown in figure 6(a) and given by equation 9.

$$\frac{\Delta m}{\Delta t} = \dot{m}_{in} - \dot{m}_{out} \tag{9}$$

Equation 9 can also be represented in an explicit form as

$$m_i^{t+\Delta t} = m_i^t + \Delta t(\dot{m}_{in} - \dot{m}_{out})_i^t \tag{10}$$

where

$$m = \rho A_x \Delta z \tag{11}$$

and

$$\dot{m} = \rho v A_x = \rho G \tag{12}$$

Since $v = G/A_x$ and $A_x = \pi d^2/4$.

For the control volume (i), the density is determined knowing the volume of the control volume.

$$\rho_i^{t+\Delta t} = m_i^{t+\Delta t}/V_i \tag{13}$$

Equation 10 introduces the new mixture mass, therefore the new phase masses will be given function of the mass fraction x, and the new volume function of the void fraction α as follow [12].

$$m_v = xm \tag{14}$$

$$m_l = (1-x)m \tag{15}$$

$$V_v = \alpha V \tag{16}$$

$$V_l = (1-\alpha)V \tag{17}$$

For a two-phase control volume and in terms of the mass fraction *x* and void fraction α, by

$$\dot{m} = \dot{m}_v + \dot{m}_l = x\dot{m} + (1-x)\dot{m} \tag{18}$$

$$V = V_v + V_l = \alpha V + (1-\alpha)V \tag{19}$$

$$\rho = \rho_v + \rho_l = \alpha\rho + (1-\alpha)\rho \tag{20}$$

Applying the conservation of energy, in terms of *thermal energy* equation, as formally derived from the more commonly used *total energy* equation to the control volume in figure 6(c), equation 21 is generated.

$$\frac{\Delta}{\Delta t}(mu) = (\dot{m}u)_{in} - (\dot{m}u)_{out} + \dot{Q}_{in} - \dot{Q}_{out} + (PAv)_{in} - (PAv)_{out} - \tau_w A_z v \quad [\text{W}] \tag{21}$$

Equation 21 can be written explicitly as

$$u_i^{t+\Delta t} = \left[(mu)_i^t + \Delta t \sum \dot{E}_i^t\right]/m_i^{t+\Delta t} \tag{22}$$

where

$$\sum \dot{E}_i^t = \left[\begin{matrix}(\dot{m}u)_{in} - (\dot{m}u)_{out} + \dot{Q}_{in} - \dot{Q}_{out} + (PAv)_{in} \\ -(PAv)_{out} - \tau_w A_z v\end{matrix}\right]_i^t \tag{23}$$

All thermodynamic properties will then be represented function of the internal energy $u_i^{t+\Delta t}$ and the density $\rho_i^{t+\Delta t}$; $f(u_i^{t+\Delta t}, \rho_i^{t+\Delta t})$. Figure 7 shows the property function diagram of the specific internal energy versus pressure.

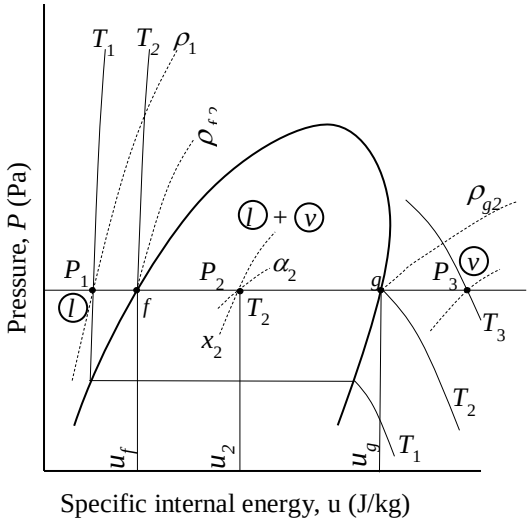

Figure 7 Pressure-specific internal energy diagram showing a sub-cooled liquid 1, a two-phase vapour plus liquid 2 and a vapour 3 state point

For the solution algorithm computer program given in figure 8, the following are used in the selected procedure.

$$m_i^{t+\Delta t} = m_i^t + \Delta t \left(\frac{\Delta m}{\Delta t}\right)_i^{t-\Delta t/2} \tag{24}$$

where

$$m_i^{t+\Delta t} = \left(\frac{\Delta m}{\Delta t}\right)_i^{t-\Delta t/2} = \frac{m_i^t - m_i^{t-1}}{\Delta t} \quad (25)$$

and

$$P_i^{t+\Delta t} = P_i^t + \Delta t \left(\frac{\Delta P}{\Delta t}\right)_i^{t-\Delta t/2} \quad (26)$$

where

$$\left(\frac{\Delta P}{\Delta t}\right)_i^{t-\Delta t/2} = \frac{P_i^t - P_i^{t-1}}{\Delta t} \quad (27)$$

Having now determined $u_i^{t+\Delta t}$ using equation 22 with $m_i^{t+\Delta t}$ as given by equation 24, the remaining thermodynamic properties may be determined as function of $u_i^{t+\Delta t}$ and $P_i^{t+\Delta t}$. That is $T_i^{t+\Delta t} = f\left(u_i^{t+\Delta t}, P_i^{t+\Delta t}\right)$ and $\rho_i^{t+\Delta t} = f\left(u_i^{t+\Delta t}, P_i^{t+\Delta t}\right)$, for a so-called sub-cooled or superheated single phase control volume (see figure 7). Using equations 22 and 24, the mass fraction for a two-phase liquid-vapour control volume is given as

$$x_i^{t+\Delta t} = \left(u_i^{t+\Delta t} - u_{f,i}^{t+\Delta t}\right)/\left(u_{g,i}^{t+\Delta t} - u_{f,i}^{t+\Delta t}\right) \quad (28)$$

where

$u_{f,i}^{t+\Delta t} = f\left(P_{sat,i}^{t+\Delta t}\right)$ and $u_{g,i}^{t+\Delta t} = f\left(P_{sat,i}^{t+\Delta t}\right)$, and the volume or void fraction $\alpha = V_l/V_v$ is given by

$$\alpha_i^{t+\Delta t} = \left(1 + SF\,\frac{\rho_{g,i}^{t+\Delta t}}{\rho_{f,i}^{t+\Delta t}}\,\frac{1-x_i^{t+\Delta t}}{x_i^{t+\Delta t}}\right)^{-1} \quad (29)$$

where SF is the slip factor, the ratio of the vapour to liquid velocities v_v/v_l. It is given by an experimentally determined correlation in terms of the vapour and liquid densities, dynamic viscosities, mass fraction and surface tension [22]. Another correlation of the void fraction is given in terms of the Martinelli parameter *X* [15] as in equations 6 and 7.

Having now the mass and void fractions (x and α), the density and the temperature at $t + \Delta t$, thermodynamic properties are now given by

$$\rho_i^{t+\Delta t} = \alpha_i^{t+\Delta t}\rho_{g,i}^{t+\Delta t} + \left(1 - \alpha_i^{t+\Delta t}\right)\rho_{f,i}^{t+\Delta t} \quad (30)$$

and

$$T_i^{t+\Delta t} = f\left(P_{sat,i}^{t+\Delta t}\right) \quad (31)$$

For a separated flow model, the left hand term of equation 21 becomes

$$\frac{\Delta}{\Delta t}(mu) = \frac{\Delta}{\Delta t}(m_v u_v + m_l u_l) = \frac{\Delta}{\Delta t}(xmu_v + (1 - x)mu_l) = \frac{\Delta}{\Delta t}\left(m(xu_v + (1-x)u_l)\right) = \frac{\Delta}{\Delta t}(mu)\} \quad (32)$$

where $u = xu_v + (1-x)u_l$

The convective energy flow terms on the right hand side of equation 21 becomes

$$(\dot{m}u)_{in} - (\dot{m}u)_{out} = x\dot{m}u_{v,in} + (1-x)\dot{m}u_{l,in} - x\dot{m}u_{v,out} - (1-x)\dot{m}u_{l,out} = \dot{m}(u_{in} - u_{out}) \quad (33)$$

And the reversible work term on the right hand side of equation 21 becomes

$$(PAv)_{in} - (PAv)_{out} = \left(P(A_v v_v + A_l v_l)\right)_{in} - \left(P(A_v v_v + A_l v_l)\right)_{out}$$
$$= \dot{m}\left[\left(P(x/\rho_v + (1-x)/\rho_l)\right)_{in} - \left(P(x/\rho_v + (1-x)/\rho_l)\right)_{out}\right]$$
$$= \dot{m}[(P/\rho_h)_{in} - (P/\rho_h)_{out}] \quad (34)$$

where

$$\rho_h = (x/\rho_v + (1-x)/\rho_l)^{-1}$$

When applying the conservation of momentum to the control volume depicted in figure 6(b) equation 35 is found

$$\frac{\Delta}{\Delta t}(mv) = (\dot{m}v)_{in} - (\dot{m}v)_{out} + (PA)_{in} - (PA)_{out} - m_i g \sin\theta - \tau A_z \ \text{[N]} \quad (35)$$

For a separated two-phase flow model, after dividing throughout by the cross sectional area A of the control volume and making use of the identities of equations 12 and 20, the momentum equation may be expressed in terms of the mass, mass flow rate, mass fraction and void fraction as given in equation 36.

$$\frac{\Delta}{\Delta t}\left[\frac{m\dot{m}}{A^2}\left(\frac{x^2}{\alpha\rho_v} + \frac{(1-x)^2}{(1-\alpha)\rho_l}\right)\right]_i = \frac{\dot{m}^2}{A_i}\left[\left(\frac{x^2}{\alpha A\rho_v} + \frac{(1-x)^2}{(1-\alpha)A\rho_l}\right)_{in} - \left(\frac{x^2}{\alpha A\rho_v} + \frac{(1-x)^2}{(1-\alpha)A\rho_l}\right)_{out}\right]$$
$$+P_{in,i} - P_{out,i} - [(\alpha\rho_v + (1-\alpha)\rho_l)g\sin\theta\,\Delta z]_i - \left[\frac{\tau_{lo}\phi_{lo}^2 A_z}{A}\right]_i \quad (36)$$

where $m = (\alpha\rho_v + (1-\alpha)\rho_l)A\Delta z$

In accordance with the concept of upwind differencing for the momentum flux term (the first term on the right hand side of equation 34 $in = i - 1$ if $\dot{m} \geq 0$ and $in = i + 1$ if $\dot{m} < 0$ and "out" always equals "in", irrespective of the flow direction.

The mass flow rate of the fluid in and around the loop, at any instance in time, is then given by summing all the control volumes around the loop from 1 to N_{tot} and noting that the pressure terms all cancel out.

$$\frac{\Delta}{\Delta t}(\dot{m}M) = \dot{m}^2 MF - G - F \quad (37)$$

Equation 37 is also explicitly given by

$$\dot{m}^{t+\Delta t} = [\dot{m}^t M^t + \Delta t(\dot{m}^2 MF - G - F)^t]/M^{t+\Delta t} \quad (38)$$

where

$$M_i^t = \sum_{i=1}^{N_{tot}}\left[m_i^t/A_i^2\left(\left(\frac{x^2}{\alpha\rho_v}\right)_i^t + \left(\frac{(1-x)^2}{(1-\alpha)\rho_l}\right)_i^t\right)\right] \quad (39)$$

$$M_i^{t+\Delta t} = \sum_{i=1}^{N_{tot}}\left[m_i^{t+\Delta t}/A_i^2\left(\left(\frac{x^2}{\alpha\rho_v}\right)_i^{t+\Delta t} + \left(\frac{(1-x)^2}{(1-\alpha)\rho_l}\right)_i^{t+\Delta t}\right)\right] \quad (40)$$

$$MF = \sum_{i=1}^{N_{tot}}\left[\frac{1}{A_i}\left(\left(\frac{x^2}{\alpha A\rho_v} + \frac{(1-x)^2}{(1-\alpha)A\rho_l}\right)_{in} - \left(\frac{x^2}{\alpha A\rho_v} + \frac{(1-x)^2}{(1-\alpha)A\rho_l}\right)_{out}\right)\right]_i \quad (41)$$

$$G = \sum_{i=1}^{N_{tot}}[(\alpha\rho_v + (1-\alpha)\rho_l)g\sin\theta\,\Delta z]_i \quad (42)$$

and

$$F = \sum_{i=1}^{N_{tot}}[\tau_{lo}\phi_{lo}^2 \wp\,(\Delta z + \Delta z_{minor})/A]_i \quad (43)$$

where Δz_{minor} is the equivalent length of pipe of the same diameter and represents the minor losses or the irreversible work done on the fluid, as a result of there being inlets or contractions, bends, outlets or expansions etc.

Having now determined the mass flow rate at any instant in time $t + \Delta t$, the control volume pressure may now be determined at the so-to-say new-new time $t + \Delta t$, equation 34 is re-arranged as

$$P_{out,i} = P_{in,i} + \frac{\dot{m}^2}{A_i}\left[\left(\frac{x^2}{\alpha A\rho_v} + \frac{(1-x)^2}{(1-\alpha)A\rho_l}\right)_{in,i} - \left(\frac{x^2}{\alpha A\rho_v} + \frac{(1-x)^2}{(1-\alpha)A\rho_l}\right)_{out,i}\right] - [(\alpha\rho_v + (1-\alpha)\rho_l)g\sin\theta\,\Delta z]_i - \left[\frac{\tau_{lo}\emptyset_{lo}^2\wp(\Delta z+\Delta z_{minor})}{A}\right]_i - \frac{\Delta}{\Delta t}\left[\frac{m\dot{m}}{A^2}\left(\frac{x^2}{\alpha\rho_v} + \frac{(1-x)^2}{(1-\alpha)\rho_l}\right)\right]_i^{t-\Delta t/2} \quad (44)$$

3.2 Property functions

Although property functions are obvious and known, it is important to highlight them in this section as used in the computer program given in the computer algorithm flow chart in figure 8. These properties are classified into three regions; the subcooled liquid region, the two-phase region and the superheated region as shown in figure 7. The property functions with respect to each region are as follow.

Subcooled liquid region, that is $x \leq 0\ and\ \alpha \leq 0$

$u = f(T), T = f(u, P), \rho = f(u, P)$

Two-phase region, that is $0 < x < 1\ and\ 0 < \alpha < 1$

$u_f = f(P), u_g = f(P), T_{sat} = f(P), \quad \rho_f = f(P), \quad \rho_g = f(P)$

Superheated region, that is $x \geq 1\ and\ \alpha \geq 1$

$T = f(u, P), \rho = f(u, P)$

Sundry property functions

$\sigma = f(T), \mu = f(T)$

4 Experimental setup

This section presents the experimental setup of the natural circulation loop used for this project and as depicted in figure 9.

Four transparent polycarbonate sight glasses are positioned at strategic points in order to visually identify two-phase flow patterns. A stainless steel expansion tank was manufactured and fitted with a glass tube level indicator in order to measure the variation in tank fill level. The tank is connected to the natural circulation loop through a valve attached to the loop return line and is placed at a height of 12 m above the lower horizontal section of the loop.

4.1 Instrumentations

Thermocouples were used to measure the temperatures of three different sections of the experimental setup, including the working fluid, the evaporator and the condenser. Twelve sheathed, K-type thermocouple probes were used to measure the working fluid temperatures at the inlet and outlet of the condenser and evaporator sections of the loop, as well as the inlet and outlet of each heat exchanger (HEs). A further eleven K-type cladded thermocouples were placed 25 mm from tip and central to each heating element in a 20 mm deep ϕ1.8 mm hole within the element to measure the temperature distribution.

In order to account for variation in the characteristics of different batches of thermocouple wire, it was decided to take the twelve sheathed thermocouples from the same roll. The accuracy was then verified by testing the thermocouples against a calibrated Isotech platinum resistance thermometer (PRT) model number 935-14-72 manufactured by ISOTECH South Africa with serial number 191069 and used with an oil bath. The PRT was calibrated on the 4th February 2013 by Rapid Instrumentation cc with certificate number RAP15738.

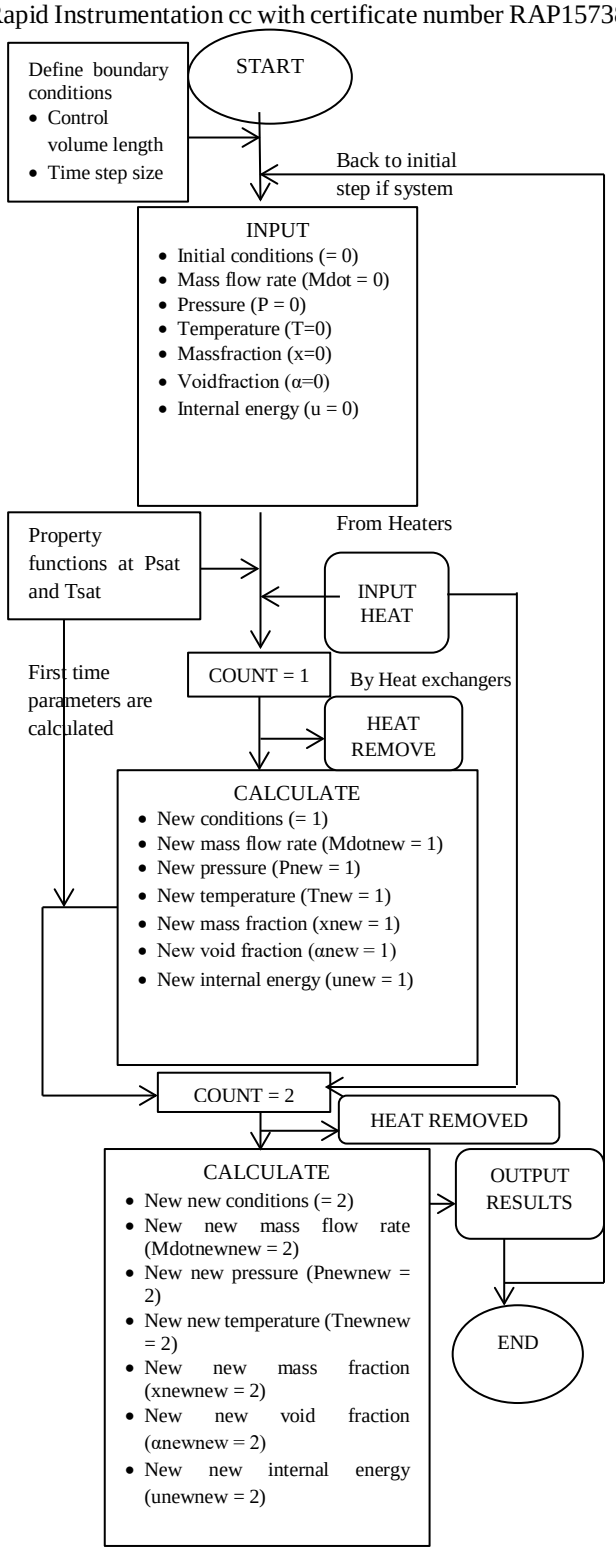

Figure 8 Computer algorithm flow chart

The mass flow rate was measured using an orifice plate and two calibrated differential pressure transducers including the HBM-PD1(Hottinger Baldwin MesstechniK type PD1) and the E&H (Endress and Hauser) Deltabar.

Both the HBM PD1, serial No 12068, with a 0.01 bar full scale reading working up to an allowable nominal operating pressure of 50 bars and the E&H Deltabar M IP66/IP67 were

used to measure the pressure difference across the orifice plate. They were calibrated using a van Essen, BETZ type 5000 water micro-manometer having a measuring range of -10 to 5000 Pa (gauge pressure) and an accuracy of ±0.2 Pa.

The temperature and mass flow rate reading instruments were connected to a 34970A Agilent data logger with serial number MY44045582. Data were logged every 1.445 s.

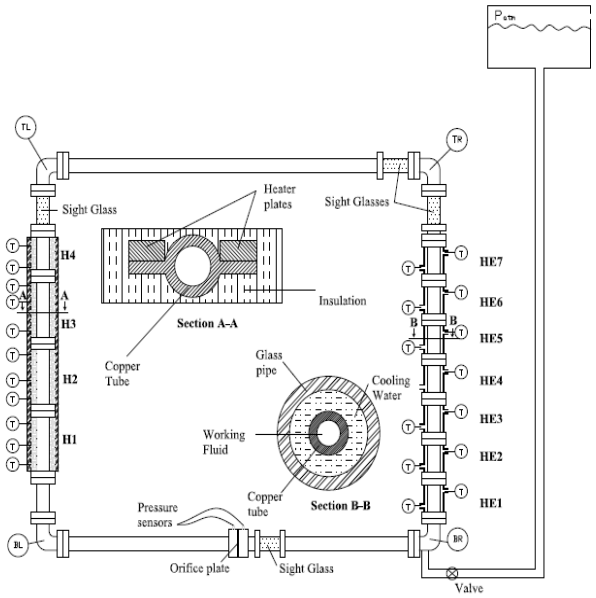

Figure 9 Experimental thermosyphon loop

4.2 Operating procedures

Before starting with the experiment, water level in the expansion tank, the room temperature and ambient pressure were measured and recorded. Leaks and electrical connections were also checked to prevent accidents.

The mass flow rate of the working fluid was measured by the pressure difference across the orifice plate while the cooling water mass flow rate through the heat exchangers (HEs) was measured manually. This mass flow rate is controlled through the use of a constant header tank as well as ball valves at the outlet of each condenser section and thus has a constant value for the duration of the experiment for each HE.

To allow heat transmission with thermal equilibrium, the same heat input procedure was used for all the experiments. During start-up, each heating element (H) was set to 30% of maximum power input. The working fluid temperature was monitored and the power input maintained until thermal equilibrium was reached. At that stage, the power input was increased to 50% for a certain duration until thermal equilibrium was reached, then the heat was increased to 70% of the full power and finally to 100%. The power supply was then switched off and the system was allowed to cool down to its initial conditions.

5 Results

In this section the results obtained from the experimental setup are compared with the theoretical results generated by the mathematical model.

5.1 Mass flow rate

Figures 10 and 11 show a comparison between the theoretically and experimentally determined mass flow rates of the working fluid for single to two-phase operating mode using the two different pressure sensors.

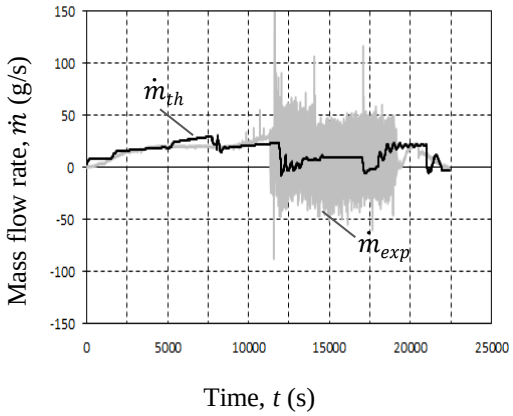

Figure 10 Experimental mass flow rate, using the HBM pressure sensor, and the theoretically predicted mass flow rate as a function of time.

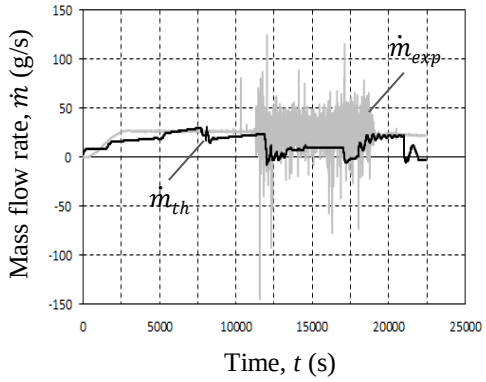

Figure 11 Experimental mass flow rate, using the E&H pressure sensor, and the theoretically predicted mass flow rate as a function of time.

The experimental mass flow rates, depicted in grey in both figures, show a steady increase in the single phase region and an oscillatory behaviour in the two phase region. The power is input progressively into the system as shown in table 1 starting with 30 % of available full power. The experimental results show that each increase of input power causes an increase in the single phase mass flow rate and temperatures as it can be seen in figures 10, 11 and 13. After 14596 s, 70 % of heat is input into the system taking the temperature profiles (T_{TL} and T_{TR}) of the top section of the loop to about 107.57 ºC coinciding with a sudden oscillatory behaviour of the mass flow rate as boiling starts. As more heat is input and once boiling is fully saturated, the mass flow rate oscillates with bigger amplitudes therefore affecting the heat transfer between the heating elements and the working fluid. The theoretical results show that mass flow rate in the single phase region also increases with time from start-up as heat is being input into the system. A slight drop in the mass flow rate is observed which is caused by the presence of bubbles in the working fluid as a result of more friction after 70 % of full power is input. For less than 100 s the mass flow rate

oscillates and stabilises when thermal equilibrium is reached again. Both mass flow rates (experimental and theoretical) in figures 10 and 11 show that when boiling start (after 70 % of full power is input) their profiles show more oscillatory behaviours and continue as such even after 100 % of power is used. The oscillations for the experimental mass flow rate have bigger amplitude than the theoretical results. This is due to the fact that instruments are more sensitive and thermal instabilities are more pronounced during the experiment. After 18000 s the power is switched off, boiling continues for about 600 s as shown in all three mass flow rate profiles, then start to cool down until the experiment or simulation is stopped. The theoretical mass flow rate closely follows the experimental profile in the single phase mode and shows a more stable profile with some oscillatory behaviour at times in the two-phase region, but nevertheless it follows a similar trend as the averaged values experimentally determined profile trend.

Table 1 Heat plate electrical power input

Power (%)	Time (s)	Heating plate 1 (W)	Heating plate 2 (W)	Heating plate 3 (W)	Heating plate 4 (W)	Total (W)
30	0	462.89	451.16	243.04	140.24	1297.33
50	7350	1080.00	1134.04	1040.38	449.54	3703.96
70	14596	2079.18	2003.58	2079.18	960.26	7122.20
100	17285	2728.30	2704.70	2767.20	1173.06	9373.26
0	22250	0.00	0.00	0.00	0.00	0.00

5.2 Pressure difference

Figure 12 shows the theoretical versus the experimental working fluid pressure difference $\Delta P = \rho g h_{tank}$ where the change in fluid density due to the rise or drop in temperature of the heating elements cause the oscillatory behaviour of the pressure difference in the loop. Both trends show that the single phase is less affected by thermal instabilities than the two-phase operating mode. This is shown in the pressures behaviours as depicted in figure 12.

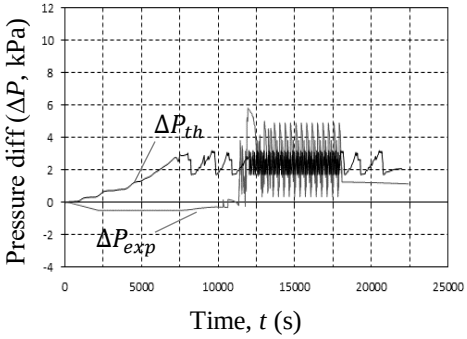

Figure 12 Experimental vs theoretical pressure difference, as a function of time

5.3 Temperature

Figure 13 presents the working fluid temperatures; (a) experimentally measured and (b) theoretically determined as functions of time, with K-type thermocouples installed in the four corners of the loop as shown in figure 9. Both results show that at each change in heat input as presented in table 1, there is an increase in working fluid temperature. After about 10000s and 70 % of full power is input into the system, the temperatures at the top of the loop (T_{TL} and T_{TR}) reach the peak that coincides with a sudden drop in mass flow rate, as boiling starts. When boiling is fully saturated, both experimental and theoretical temperature profiles in the top of the loop follow a similar trend around the saturation line.

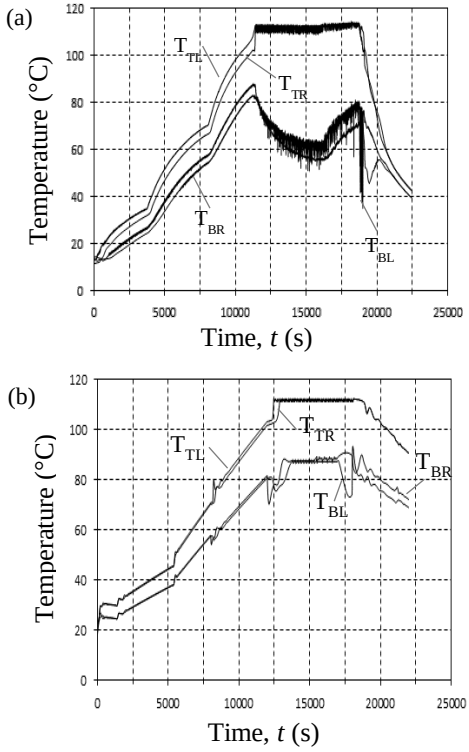

Figure 13 Working fluid temperatures as function of time: (a) Experimental, (b) Theoretical

The temperature profiles of TBL and TBR however show that boiling did not occur due to heat removed as the fluid passes the condenser section. TBR shows a more chaotic

oscillatory behaviour of amplitudes up to 40 °C due to mixing of warn and less dense fluid from the condenser section and cool and more dense water from the expansion tank generating positive and negative differences in pressure. After 18000 s, the power is switched off and both profiles show that all temperatures decrease with time until the experiment and simulation are stopped.

6 Discussions

Information collected through the literature review shows that the basic approach in theoretically simulating the single and two-phase flow of a natural circulation loop using the separated two-phase flow model is to discretize the loop into a series of parallel one-dimensional axially symmetrical control volumes where the two-phase flow is treated with the liquid and gas phases considered separately. After the loop is discretized, conservation equations of mass, momentum and energy are applied and corresponding correlations used.

The experimental setup was conducted on an existing loop designed by Sittmann [19]. The loop was recommissioned, instrumented and prepared for the experiments. More than a dozen of test-runs were conducted on the loop, lasting up to 4 hours each, with data logging occurring every 1.445 seconds and electrical power input into the system in steps of 30, 50, 70 and 100 per cent of full power.

A numerical model was developed and created in Q-Basic64 to simulate the loop thermosyphon and predict the working fluid mass flow rate, temperatures and pressure difference behaviours during the single and two-phase operating modes.

An important objective of the experimental work was to assist in determining the accuracy of the theoretical model. Figures 10, 11 and 12 show the theoretical results superimposed on the experimental results of the mass flow rate and pressure difference, and figure 13 shows a comparison of the working fluid temperatures between the two results. From the four figures it can be seen that theoretical results correspond reasonably well with the experimental results. However the experimental mass flow rates show more oscillatory behaviour in the two-phase region, caused by instabilities occurring during boiling and the sensitivity of the pressure sensors than the theoretical model. The theoretical results corresponds well with the average values for the mass flow rate read with the HBM pressure sensor and is slightly offset from the average line for the E&H pressure sensor. The experimental pressure difference profile however corresponds more accurately in both the single and two-phase mode with the theoretically predicted values.

Regarding the temperature profiles, TBL of the experimental results shows a more oscillatory behaviour than the theoretical because of its location, where low dense warm water from the condenser mixes with higher density cool water from the tank. It therefore generates more thermal instabilities at that location in the loop as depicted in the profile behaviour of TBL of figure 13(a). The other temperatures profiles (for both theoretical and experimental results) correspond relatively well.

7 Conclusion and recommendations

In conclusion, the theoretical investigations using the separated two-phase model as presented in section 5 provides relatively accurately calculated thermo-fluid parameters of the natural circulation loop with respect to the experimentally predicted values. This is shown in the behaviours of the mass flow rate, pressure and temperature profiles given in figures 10, 11, 12 and 13. Theoretical profiles follow similar trends as the experimental, thereby validating the use of the separated two-phase flow model for modelling natural circulation loops. Although there are some discrepancies in the two-phase region for the mass flow rate that requires improvements in capturing thermal instabilities. The use of the separated two-phase model for modelling natural circulation loops makes a strong argument for design purposes.

The numerical model using the separated two-phase flow can be confidently recommended for use in future two-phase flow studies. However an add-on program for thermal instabilities analysis should be developed in order to capture more accurately chaotic transient behaviours.

References

[1] IAEA. Heat Transport and afterheat removal for gas cooled reactors under accident conditions. TECDOC-1162, IAEA, Vienna, 2000.

[2] K. Hibi, H. Ono, and T. Kanagawa. Integrated modular water reactor (IMR) design. *Nuclear Engineering and Design*, 230(1-3):253–266, 2004.

[3] IAEA. Safety related terms for advanced nuclear plants. TECDOC-626, IAEA, Vienna, 1991.

[4] D. Reay, and P. Kew. *Heat Pipes: Theory, Design and Applications*. 5th Edition, Butterworth-Heinemann, Oxford, 2006.

[5] R. Greif, Y. Zvirin, and A. Mertol. The transient and stability behaviour of a natural convection loop. *Journal of Heat Transfer*, 101(4):684-688, 1979.

[6] M. Gordon, E. Ramos, and M. Sen. A one-dimensional model of a thermoshon with known wall temperature. *International Journal of Heat and Fluid Flow*, 8(3): 177-181, 1987.

[7] O. Salazer, M. Sen, and E. Ramos. Flow in conjugate natural circulation loops. *Journal of Thermophysics and Heat Transfer*, 2(2):180-183, 1988.

[8] M. Sen, D. A. Pruzan, and K. E. Torrance. Analytical and experimental study of steady-state convection in a double-loop thermosiphon. *International Journal of Heat and Mass Transfer*, 31(4):709-722, 1988.

[9] J. C. Chato. Natural convection flows in parallel-channel systems. *Journal of Heat Transfer*, 85(4): 339-345, 1963.

[10] B. J. Huang, and R. Zelaya. Heat transfer behaviour in a thermosyphon loop. *Journal of Heat Transfer*, 110(2): 487-493, 1988.

[11] K. P. Halliman, and R. Viskanta. Dynamics of a natural circulation loop: analysis and experiments. *Heat Transfer Engineering*, 7(3-4):43-52, 1986.

[12] P. K. Vijayan, S. K. Metha, and A. K. Date. On the steady-state performance of natural circulation loops. *International Journal of Heat and Mass Transfer*, 34(9):2219-2230, 1991.

https://doi.org/10.69694/2309-8988/v34a9

[13] R. Grief. Natural circulation loops. *Journal of Heat Transfer*, 110(4b):1243-1258, 1988.

[14] A. K. Nayak, and P. K. Vijayan. Flow instabilities in boiling two-phase natural circulation systems: A review. *Science and Technology of Nuclear Installations*, 2008.

[15] P. K. Vijayan, and A. K. Nayak. Introduction to instabilities in natural circulation systems, Lecture Notes for T-06, *IAEA Training Course on Natural Circulation Phenomena and Passive Safety Systems in Advanced Water-Cooled Reactors*, ICTP, Trieste, Italy, 17-21 May 2010.

[16] S. Bhattacharyya, D. N. Basu, and P. K. Das. Two-phase natural circulation loops: A review of the recent advances. *Heat Transfer Engineering*, 33(4-5):461–482, 2012.

[17] R. Dobson. Transient response of a closed loop thermosyphon. *R&D Journal*, 9(1):32-38, 1993.

[18] J. Ruppersberg. *Transient and scaling effects in single and two phase natural circulation thermosyphon loops suitable for the reactor cavity cooling of a pebble bed modular reactor*. MScEng thesis, Department of Mechanical and Mechatronic Engineering, Stellenbosch University, South Africa, 2007.

[19] I. Sittmann. *Inside-pipe heat transfer coefficient characterisation of a one third height scale model of a natural loop suitable for reactor cavity cooling system of the PBMR*. MScEng thesis, Department of Mechanical and Mechatronic Engineering, Stellenbosch University, South Africa, 2010.

[20] P. B. Whalley. *Boiling Condensation and Gas-Liquid Flow*. Clarendon Press, Oxford, 1987.

[21] Van P. Carey. *Liquid-Vapor Phase-Change Phenomena*. Taylor & Francis, 1992.

[22] S. M. Ghiaasiaan. *Two-phase Flow, Boiling and Condensation in Conventional and Miniature Systems*. Cambridge University Press, New York, 2007.

[23] P. K. Vijayan, A. K. Nayak, D. Saha, and M. R. Gartia. Effect of loop diameter on the steady state and stability behaviour of single-phase and two-phase natural circulation loop. *Science and Technology of Nuclear Installations*, 2008.

https://doi.org/10.69694/2309-8988/v34a9